*32nd EPS Conference on Plasma Phys. Tarragona, 27 June - 1 July 2005 ECA Vol.**29C**, P-4.019 (2005)*

The 3D modelling of dust particle transport in tokamak plasmas with the newly developed DUSTT code

A.Yu. Pigarov[1,4], T.K. Soboleva[2,4], S.I. Krasheninnikov[1], T.D. Rognlien[3]

[1] *Center for Energy Research, University of California at San Diego, La Jolla, CA, USA*
[2] *UNAM, Mexico, D.F., Mexico*
[3] *Lawrence Livermore National Laboratory, Livermore, CA, USA*
[4] *Also with Institute of Nuclear Fusion, RRC "Kurchatov Institute", Moscow, Russia*

I. Introduction. Dust particulates of 10nm-100μm in size (as well as flakes and loose co-deposited layers of larger size, up to ~1 mm) are unavoidably present in all fusion devices [1]. The dust can be generated during tokamak operation due to strong plasma-material surface interactions. The special attention of fusion community to dust is because of its potentially serious threat to the safety of next-step fusion devices. Moreover, recent experiments [1] and theoretical estimates [2] have indicated that dust particles can provide an important source of impurities in the tokamak plasma. We have developed the DUST Transport (DUSTT) code and report here results on the dust dynamics and transport in various tokamaks as well as on the possible effect of dust on divertor plasma profiles.

II. Model for dust particle transport in tokamak plasma. The dynamics of a test dust particle is governed by a set of coupled differential equations for temporal evolution of radius-vector **r**, velocity vector **v**, dust radius R_d, charge Z_d, and temperature T_d. The equations of motion are: $d\mathbf{r}/dt=\mathbf{v}$, $M_d d\mathbf{v}/dt=\mathbf{F}_d(\mathbf{r},\mathbf{v})$, where $\mathbf{F}_d=\mathbf{F}_{fric,ion}+\mathbf{F}_{fric,n}-eZ_d\mathbf{E}_{plasma}+M_d\mathbf{g}$ is the resulting force vector, $M_d=4/3\ \pi R_d^3\rho_d$ is the dust mass, **g** is the acceleration due to gravity. The trajectory is also affected by collisions of the dust particle with material surfaces and with plasma micro-turbulence. We use the simplified expressions for charge $Z_d=\lambda T_e R_d/e^2$ and friction forces: $\mathbf{F}_{fric,ion}=\zeta_{fric,ion}\Gamma_{ion}(\mathbf{V}_{ion}-\mathbf{v})A$, $\mathbf{F}_{fric,n}=\zeta_{fric,n}\Gamma_n(\mathbf{V}_n-\mathbf{v})A$, where $\mathbf{V}_{ion}$ and $\mathbf{V}_n$ are the flow velocities of plasma ions and neutrals, and $A=\pi R_d^2$. Coefficients λ and ζ are fits to the results of PIC simulations in [3]. The radius R_d decreases in time as $\rho_d dR_d/dt=-m_s\Gamma_s$, where specific fluxes Γ_s of particles with mass m_s from the dust are due to physical and chemical sputtering, and radiation-enhanced and thermal sublimation. Evolution of T_d obeys $d[C_{pd}M_dT_d]/dt=4\pi R_d^2\{q_{plas}-\varepsilon_d\sigma_{sb}(T_d^4-T_w^4)-G_s\Gamma_s\}$, where q_{plas} is the heat flux applied to the dust surface, σ_{sb} is Stefan-Boltzmann constant, T_w is the wall temperature, $G_s\Gamma_s$ is the heat flux associated with kinetic energy of sputtered and sublimated material. The heat q_{plas} absorbed by dust is due to (i) kinetic energy transfer from neutral and plasma particles, and (ii) release of plasma potential energy. We assume dust particle matter density ρ_d, specific heat C_{pd}, black-body emissivity ε_d, and vapor pressure parameters are the same as for the originating material surface (i.e. for carbon, here). The DUSTT code operates on a 2D curvilinear non-uniform mesh based on MHD equilibrium. Plasma and neutral-gas parameters are calculated by the edge transport code UEDGE with multi-ion diffusive-and-convective model for anomalous cross-field transport [4]. DUSTT performs tracking of test dust particles using the force $\mathbf{F}_d$, particle and energy fluxes, and other parameters based on UEDGE solution for edge plasma. DUSTT employs an explicit solver for a system of differential equations and uses a Monte Carlo method to simulate collisions. The input parameters for a trajectory are initial radius r_{d0}, temperature T_{d0}, velocity v_{d0}, birth point coordinates, and polar angle μ_{d0} from surface normal.

III. Dust dynamics in NSTX and DIII-D tokamaks. Examples of trajectories of dust particles are given in Fig.1. They were calculated with DUSTT based on the plasma back-

ground simulated with UEDGE by matching the experimental data for NSTX L-mode shot 109033. On upper panels, we displayed two 3D plots (in {r, z, θ} space, where r and z are the radial and vertical coordinates, θ is the toroidal angle) for trajectories originated in the strike point on the inner (left upper panel) and outer (right) divertor plates. In both cases: v_{d0}=1m/s, μ_{d0}=30°, r_{d0}=1μm. The corresponding 2D traces of these trajectories on the UEDGE mesh are shown on bottom panels. As seen, the particles travel a long way, >0.5 m poloidally, until mostly evaporated (calculations stop when particle radius decreases tenfold, i.e. the corresponding loss of mass is 10^{-3}). These trajectories are elongated in the toroidal direction, which can be understood by comparing the increments in toroidal $\delta L_\theta=\int|v_\theta|dt \approx\langle r\rangle*\Delta\theta$ and poloidal $\delta L_p=\int[v_r^2+v_z^2]^{1/2}dt \approx[\Delta r^2+\Delta z^2]^{1/2}$ lengths. In fact, the trajectory starting in the outer divertor (right panels), $\langle r\rangle\approx0.7$, $\Delta r\approx0.2$, $\Delta z\approx0.2$m, and $\Delta\theta\approx1.3$ has $\delta L_\theta/\delta L_p \approx3$. The trajectory elongation in the θ-direction is confirmed by some experiments. Another important feature is that near the divertor plates the preferential toroidal direction of dusts flight depends on the direction of parallel plasma flow which is different on the inner and outer plates. In Fig.1 (left top), the dust particle moves in negative θ while in the inner divertor, and it reverses its θ direction when it reaches the outer divertor. Such behavior is due to the dominance of ion friction force in the dust particle dynamics. Comparing left and right top plots, we find that in the recycling region near divertor plates, the particles move in the opposite toroidal directions. Using DUSTT, we also analyzed trajectories for DIII-D L-mode shot 105517.The trajectory originates from the outer divertor strike point,v_{d0}=10m/s,μ_{d0}=30°,r_{d0}=1μm, as shown on Fig.2, left upper panel. The evolution of T_d and M_d/M_{d0} along the trajectory ($L\equiv L_p=\int_o^t[v_r^2+v_z^2]^{1/2}dt$) are displayed in the upper right. As seen, when particle travels through the hot and dense regions, it heats up to sublimation level >2500K and cools in the weak plasma regions. The particle (bottom right) and heat (bottom middle) loads on dust surface are shown along the trajectory (fine steps on these curves are due to transitions in the UEDGE mesh). Comparing the plots for T_d and incident heat flux q_{plas}, one sees that after "heat pulses" at $L/L_{max}\approx0.05$ and ≈0.37, the particle is continuously cooling by black-body

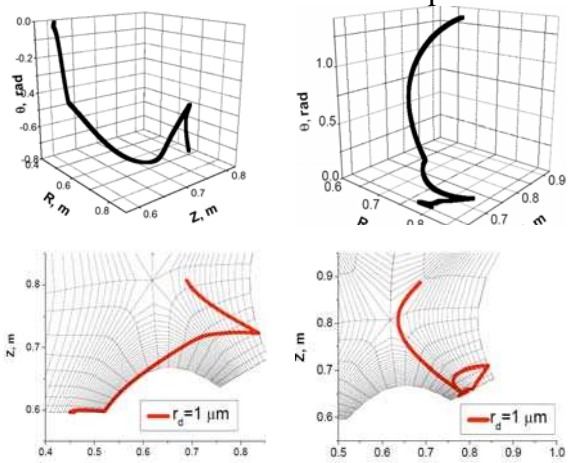

Fig.1

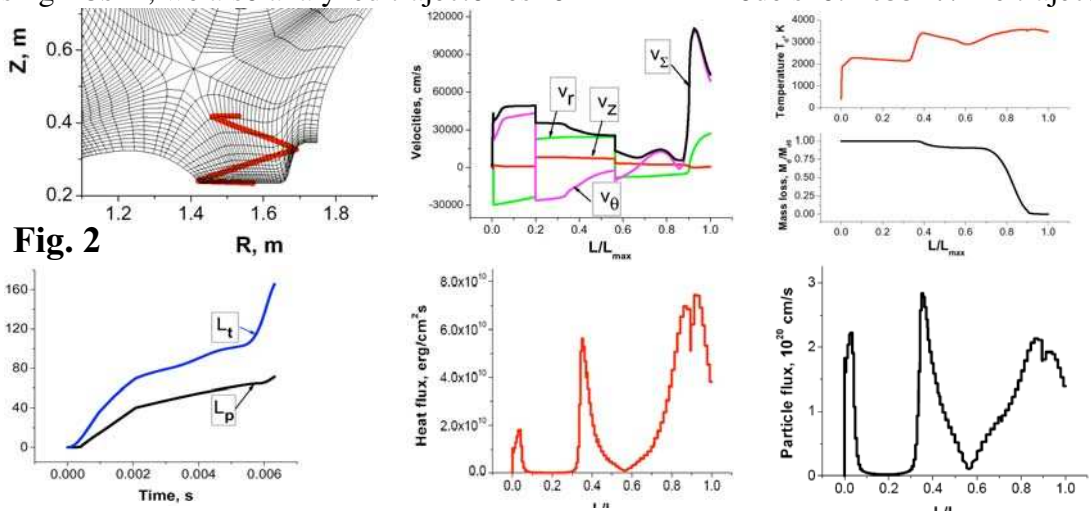

Fig. 2

radiation, however, there is not enough time for this particle to substantially cool down as it again encounters the hot plasma upon reflection from the end plate. Velocity $v_\Sigma=|\mathbf{v}|$ and components are given in the upper middle panel. The dust particle is accelerated by plasma to large velocities v_Σ>100m/s and gains energy $E_d=M_d v_\Sigma^2/2$>1GeV. The cruise speed on trajectory is few hundreds m/s, while at the end, the velocity attains ~1km/s since acceleration $\sim F_{fric,ion}/M_d \propto 1/R_d$ strongly increases due to intense decrease in the particle size and mass. The total ($L_t=\int|\mathbf{v}|dt$) and poloidal (L_p) distances traveled by a particle are displayed on the bottom left versus time into the trajectory. The characteristic time of dust particle residence in the plasma is several ms. As discussed in [2], dust particles levitating inside the plasma sheath nearby divertor plates can accelerate to 10 m/s along the magnetic field and leave the sheath region due to diffuse collisions with corrugated surface. Here, for simplicity, we do not simulate dusts behavior inside the sheath; instead, we input the v_{d0}, μ_{d0} and employ reflection boundary conditions. The left panel on Fig.3 displays four trajectories for 1055017 DIII-D, $\mu_{d0}=30^o$, $r_{d0}=10\mu$m and different initial velocities: 10^1(A), 10^2(B), 10^3(C), 10^4(D) cm/s. For large $v_{d0}\geq10^4$cm/s the trajectory (D) is almost the straight line from plate to core, whereas for smaller v_{d0} the trajectories depend largely on $\mathbf{F}_d$. For each trajectory, we also showed (right panel) the variation of M_d and T_d.

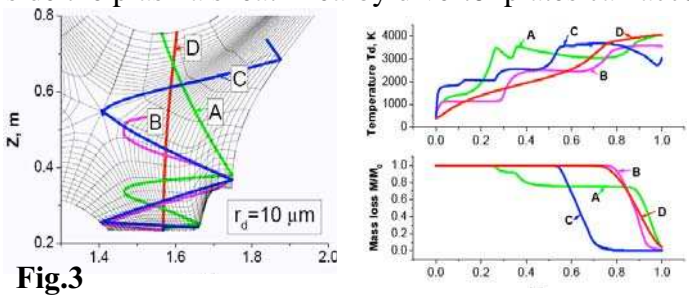

Fig.3

IV. Trajectories of dust particles in ITER. We use UEDGE to obtain the profiles of plasma parameters and flows for ITER-FEAT (114 MW input to the SOL, D/T burning plasma) and use DUSTT code to calculate the dust particle trajectories. On Fig. 4, we display three trajectories for $v_{d0}=10^2$ (A, pink), 10^3 (B, blue), and 10^4 (C, red) cm/s calculated for $r_{d0}=1\mu$m (left panel) and $r_{d0}=10\mu$m (right), which originate from the strike point at the inner divertor plate at almost normal direction $\mu_{d0}=1^o$. Because of large heat flux, these particles are mostly burned up in the divertor plasma. However, the dusts significantly advance the impurity ionization source from the plate toward the core. The trajectories originating from the dome in the private flux region are shown on Fig.5 (left) for $r_{d0}=1\mu$m. The corresponding variation of dust temperature and mass are displayed in the middle. As seen, even 1μm particles from this origin can efficiently penetrate toward the X-point. Near X-point the particle (C) mostly moves in the toroidal direction, $L_t/L_p\approx5$ (right panel) because of small pitch angle of magnetic field lines. On Fig.6 we present the group of trajectories, $v_{d0}=10^2$(A), 10^3(B), 10^4(C) cm/s, $\mu_{d0}=1^o$, $r_{d0}=1\mu$m, originated from the chamber wall at the inner (left panel) and outer (right) mid-planes. As seen, the penetration of low-v_{d0} particles in the radial direction is more efficient on the inner side rather then on the outer side of the chamber. The effect of toroidal curvature is one possible explanation for this behavior. In fact, the plasma flows of ~10km/s at the mid-plane are mostly in the toroidal (θ) direction. Due to friction force, dust particles (A,B) are largely entertained by plasma flow, and the resulting centrifugal

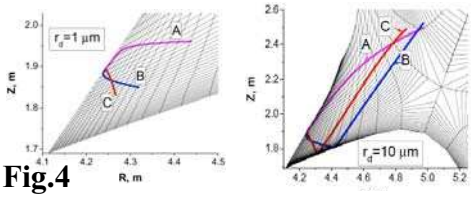

Fig.4

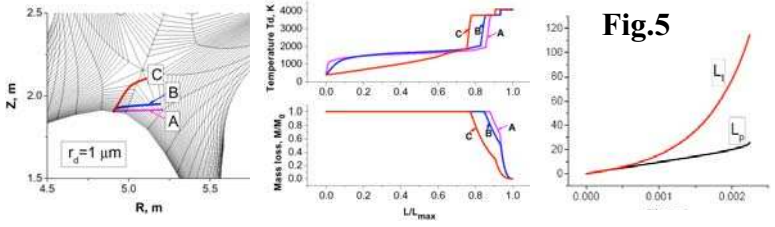

Fig.5

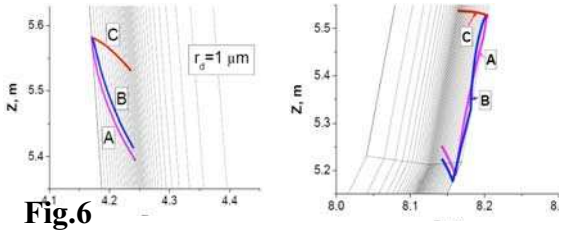

Fig.6

force pushes the particle toward the core on the inboard and toward the wall on the outboard side. The particles have more wall collisions at the outboard.

V. Estimate of the effect of dust particles on divertor plasma profiles. Dust particles are capable of penetrating much farther into plasma in comparison to single impurity atoms and ions. In order to estimate the effect of enhanced penetration of impurities due to dust evaporation on divertor plasma, we performed a series of UEDGE runs [4] in which we scan the parameters that affect the impurity atom transport. UEDGE incorporates the simple diffusive gas model with coefficient $D_{imp}=2T_{imp}/[m_{imp}\nu_{imp}]$,where $m_{imp},T_{imp},\nu_{imp}$ are the mass, temperature, and collision frequency and $T_{imp}=\alpha T_c+(1-\alpha)T_i\eta$ is a fitting parameter. Normally, we use α=0.95-0.99, η=0.9, $T_c\approx$0.1eV that gives T_{imp}=0.2-0.6eV near material surfaces which is roughly in the energy range for sputtered particles or dissociation products. The results for DIII-D shot 105517 are presented in Fig.7. Here, the contour plots for plasma temperature T_e (top panels) and C^+-ion density (bottom panels) for two cases: α=0.99 (left) and α=0.8 (right), in which D_{imp} differs by ≈30 times. As seen

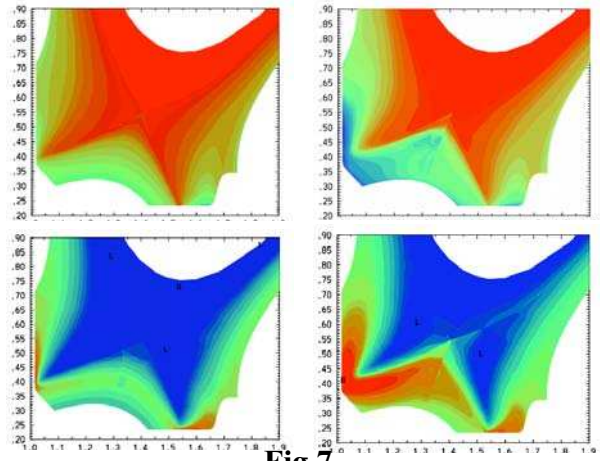

Fig.7

(top left), for α=0.99, both inner and outer divertors are attached and the temperature attained at the inner strike point $T_{e,X,in}$ is rather high, ≈7eV. The decrease in α down to only 0.8 results in substantial (~3x) decrease in T_e in both divertors and even causes detachment of the inner leg, $T_{e,X,in}$<1eV (top right). An improved penetration of impurity neutrals changes the C^+ density profile (Fig.7, bottom panels) by moving it closer toward the core plasma. The concentrations of impurity ions near separatrix are by 2-3 orders of magnitude larger in the case α=0.8 than in the low penetration case α=0.99.

VI. Conclusions. Our simulations of dust dynamics in the realistic tokamak plasma environment with DUSTT and UEDGE codes showed that dust particles are very mobile and accelerate to large velocities due to ion friction force (cruise speed >100 m/s). The DUSTT code is capable of reproducing many features of recent dust-related experiments in tokamaks. The evaporation of dusts can significantly advance the impurity ion source toward the core plasma. As follows from our UEDGE simulations, if dust transport causes enhanced penetration of impurity neutrals into plasma, then an improved penetration can substantially decrease the divertor temperature, increase core contamination with impurities, and even detach deeply the inner divertor leg. Our results motivate more detailed experimental and theoretical studies of dust production, dynamics, and transport.

References:

[1] Materials of "Dust in Fusion Plasmas" Workshop (Napa, USA, 2005) available at http://maemail.ucsd.edu/~dust/; [2] S. I. Krasheninnikov et al, Phys. Plasmas **11** (2004) 3141; [3] I. H. Hutchinson, Plasma Phys. Control. Fusion 47 (2005) 71; [4] A. Yu. Pigarov et al, J. Nucl. Mater. **313** (2003) 1076; **337** (2005) 371.